JGR Space Physics

RESEARCH ARTICLE
10.1029/2023JA032138

Key Points:

- Persistent dynamic pressure and excited Ultra-Low Frequency waves caused the electron dropout during the initial phase and the onset of the main phase
- Local acceleration of electrons induced by chorus during the main phase and recovery phase can explain the interruption of the dropout
- Special conditions in the magnetic cloud and the sheath dominate the balance of the acceleration and loss of the radiation belt electrons

Correspondence to:
P. Zuo and Z. Zou,
pbzuo@hit.edu.cn;
zyzou@must.edu.mo

Citation:
Wei, J., Zou, Z., Zuo, P., Ni, B., Ruan, M., & Feng, X. (2024). Commencement and interruption of relativistic electron dropout in the heart of the outer radiation belt induced by a magnetic cloud event. *Journal of Geophysical Research: Space Physics*, *129*, e2023JA032138. https://doi.org/10.1029/2023JA032138

Received 4 OCT 2023
Accepted 12 JAN 2024

Commencement and Interruption of Relativistic Electron Dropout in the Heart of the Outer Radiation Belt Induced by a Magnetic Cloud Event

Jiayun Wei[1,2], Zhengyang Zou[3], Pingbing Zuo[1,2], Binbin Ni[4], Mengsi Ruan[1,2], and Xueshang Feng[1,2]

[1]Shenzhen Key Laboratory of Numerical Prediction for Space Storm, Institute of Space Science and Applied Technology, Harbin Institute of Technology, Shenzhen, People's Republic of China, [2]Key Laboratory of Solar Activity and Space Weather, National Space Science Center, Chinese Academy of Sciences, Beijing, People's Republic of China, [3]State Key Laboratory of Lunar and Planetary Sciences, Macau University of Science and Technology, Macao, People's Republic of China, [4]Department of Space Physics, School of Electronic Information, Wuhan University, Wuhan, People's Republic of China

Abstract We analyze and discuss the commencement and interruption of the relativistic electron dropout in the heart of the outer radiation belt ($L^* = 4$–5) induced by a typical magnetic cloud (MC) event. This MC event impinged the Earth's magnetosphere on 31 October 2012 and caused a moderate geomagnetic storm with a special prolonged initial phase lasting for >13 hr. The relativistic electrons phase space density (PSD) dropout commenced at $L^* > 5$ during the initial phase. The PSD dropout penetrated deep beyond the heart of the radiation belt (reached $L^* < 4$) at the onset of the main phase, while it was partially enhanced with a local PSD maximum around $L^* = 4.5$, thus causing the interruption of the PSD dropout. The dropout became pronounced at $L^* > \sim 4.7$ while the local PSD maximum was maintained throughout the main phase. During the recovery phase, the dropout totally disappeared at $L^* < 5.5$ with relativistic electron PSD gradually recovering to pre-event level or higher. Further investigations on solar wind parameters and plasma waves give evidence that (a) persistent high dynamic pressure and the triggered Ultra-Low Frequency waves contribute to the dropout of electrons to interplanetary space during the initial phase and the onset of the main phase; (b) local acceleration by chorus waves during the main phase and recovery phase could explain the interruption of the dropout. Our study underlines the persistent high dynamic pressure competing with intense chorus waves in triggering the commencement and interruption of the relativistic electrons PSD dropout in the heart of the outer radiation belt.

1. Introduction

Interplanetary coronal mass ejections and corotating interaction regions, can interact with the Earth's magnetosphere and trigger geomagnetic storms or substorms, which play an important role in the population of particles trapped by the Earth's radiation belt (Borovsky & Denton, 2006; Morley et al., 2010; D. L. Turner et al., 2019; Zou et al., 2020). One of the drastic changes in radiation belt particles is electron flux or phase space density (PSD) dropout events, in which electrons can decrease by several orders of magnitude on timescales less than a few hours (Moya et al., 2017; Reeves et al., 2013; D. L. Turner et al., 2013; Zhao & Li, 2013). It is suggested that radiation belt electron flux dropout is usually caused by both the adiabatic effects and nonadiabatic effects simultaneously. The former can be regarded as the "fake loss." When the geomagnetic field in the radiation belt is weakened (enhanced) by the increase (decrease) in the ring current during the storm main phase (recovery phase), the observed electron flux at a fixed energy shows depletion (growth) by conserving their first and third invariants. Comparably, the rapid loss by the nonadiabatic effects is called the "true loss," which is commonly considered to occur by one or a combination of two mechanisms: (a) loss into the Earth's atmosphere due to pitch angle scattering via wave-particle interactions with various plasma waves, such as electromagnetic ion cyclotron (EMIC) waves; and (b) loss out of the magnetopause by the magnetopause shadowing effect combined with outward radial transport when the total configuration of the geomagnetic field is compressed by solar winds (Shprits et al., 2006; Turner & Ukhorskiy, 2020; Turner et al., 2012, 2014). To remove most of the ambiguity due to purely adiabatic effects, the "true loss" of radiation belt electrons is separated from their adiabatic variations, recent studies usually converted the electron fluxes from spatial coordinates to PSD coordinates. The results show that the large-scale rapid loss at high L^* (the drift shell in adiabatic invariant coordinate) is extremely correlated with persistent strong dynamic pressure and intense Ultra-Low Frequency (ULF) waves (e.g., Hao

et al., 2017; Turner & Ukhorskiy, 2020; Zhang, Li, Thorne, Angelopoulos, Ma, et al., 2016; Zou et al., 2020), while the local rapid loss of relativistic electrons is usually caused by EMIC-induced wave-particle interactions in dense plasma areas (e.g., Ni et al., 2015; Su et al., 2017; Xiang et al., 2017).

Compared with the electron PSD loss processes, one of the most remarkable acceleration mechanisms of relativistic electrons in Earth's radiation belt is the energy resonance dominated by the whistler mode chorus. Whistler-mode chorus waves are naturally generated electromagnetic waves excited by anisotropic electrons with two typical wave frequency bands, that is, the upper band and the lower band, with a gap of approximately half of the electron gyrofrequency (e.g., Gao et al., 2016; Li et al., 2011, 2019). It has been widely reported that chorus waves are mostly observed near the geomagnetic equator and can preferentially accelerate ~100 keV electrons to relativistic electrons at larger pitch angles through efficient energy diffusion in the heart of the outer radiation belt (e.g., Chen et al., 2007; Horne, 2005; Reeves et al., 2013; Summers et al., 2002). This acceleration process can drastically change the spatial distribution of the radiation belt electrons as well as their spectrum within a few hours (Allison et al., 2021; Li et al., 2014; Ma et al., 2016).

Recently, Zou et al. (2020) reported a two-step dropout event occurring in the initial phase and the main phase of a geomagnetic storm induced by a typical magnetic cloud (MC) event. Detailed analysis suggests that persistent high dynamic pressure combined with ULF wave-induced outward diffusion can account for electron dropout, while the chorus wave potentially leads to a partial recovery of the electron PSD during the beginning of the main phase. In the present study, we provide another event of electron variations induced by a MC event in which the relativistic electron PSD dropout occurred and was interrupted in the heart of the Earth radiation belt ($L^* = 4$–5) by using observations from both Van Allen Probes from 31 October to 2 November 2012. Compared with the partial recovery of the electron PSD in Zou et al. (2020), a remarkable local maximum of the PSD appeared at approximately $L^* = 4.5$ and was maintained for ~15 hr until the PSD in the entire range of $L^* > 4$ was pumped up to the pre-event level or higher during the recovery phase. The local acceleration of relativistic electrons significantly interrupted the dropout of the electron PSD process. Further analysis suggests that the excited chorus waves account for acceleration. Our study underlines the important roles of the structures of the dynamic pressure as well as the southward magnetic fields that trigger the substorm in MCs and the sheath region that would potentially trigger the commencement and interruption of relativistic electron dropout in the heart of the outer radiation belt.

2. Data

In this study, we used the pitch angle-resolved electron flux from the Relativistic Electron Proton Telescopes (REPT) (Baker et al., 2013) and Magnetic Electron Ion Spectrometers (MagEIS) (Blake et al., 2013) instruments from the Energetic particle Composition and Thermal plasma suite (RBSP-ECT) (Blake et al., 2013) as well as the electric field and magnetic field observations from the Electric and Magnetic Field Instrument Suite and Integrated Science (EMFISIS) (Kletzing et al., 2013) onboard both the Van Allen Probe -A and -B spacecraft. The electron fluxes are converted to PSD with three fixed adiabatic invariants (μ, K, and L^*) using the TS04 geomagnetic field model (Tsyganenko, 2005), by using the method in previous studies (e.g., Ni et al., 2009). In addition, the geomagnetic indices (e.g., SymH and AE) at a 1-min resolution obtained from the OMNI database, the magnetic field data from the Magnetic Field Investigation (MFI) (Lepping et al., 1995) and plasma data from the Solar Wind Experiment (SWE) (Ogilvie et al., 1995) on board the WIND spacecraft to identify solar wind disturbances.

3. Observations

Figure 1 shows an overview of the MC event and the driven geomagnetic storm, which were observed by WIND from 31 October to 2 November 2012. An interplanetary shock induced by this MC was detected at 14:30 UT on 31 October and labeled by "S." After IP shock, the sheath region appeared with a strong magnetic field intensity (Figures 1a and 1b), and persistent high dynamic pressure (Figure 1h), until the arrival of the MC body at 23:30:45 UT on 31 October (the first red vertical line). This typical MC can be identified by strong magnetic field, large-scale magnetic field rotation and lower proton temperature. The storm sudden commencement (SSC) occurred at 15:40 UT on 31 October (marked with the first vertical blue line in Figure 1i) triggered by the IP shock. Following the SSC, the SymH stayed around a high value for more than 13 hr until it declined to the pre-event level (approximately ~8 nT, the dashed horizontal line in Figure 1i) at 04:44 UT. This prolonged initial phase covered

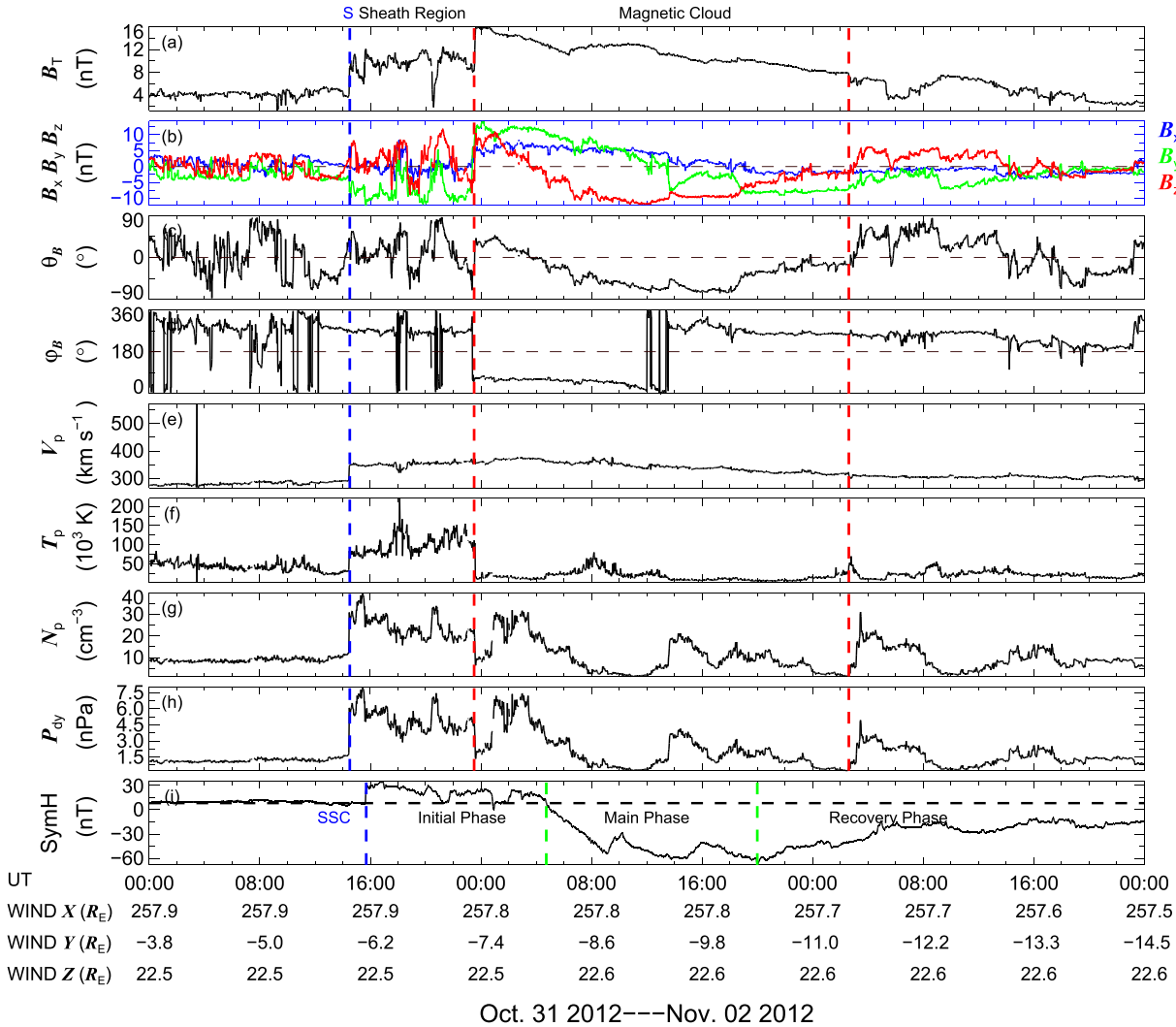

Figure 1. A typical magnetic cloud (MC) event observed by WIND from 31 October to 2 November 2012. From top to bottom, panels are the (a) magnetic field intensity, (b) three components of the magnetic field in Geocentric Solar Ecliptic (GSE) coordinates, (c) latitudinal angle, (d) azimuthal angle, (e) proton velocity, (f) proton temperature, (g) number density, (h) solar wind dynamic pressure, and (i) SymH index. The red vertical dashed lines show the beginning and end times of MC. The MC-driven interplanetary shock is represented by the first blue vertical dashed line labeled by "S." In panel (i), the black horizontal dashed line represents the average value of the SymH before storm sudden commencement, and the beginning and end times of the storm main phase are marked with two green vertical dashed lines.

an entire orbital period of Van Allen Probes (~9 hr), providing a good opportunity to investigate the change in the radiation belt electron fluxes after the IP shock without the Dst effect in the storm initial phase. The main phase of the moderate geomagnetic storm could be identified with SymH reaching a minimum value of −68 nT at 20:00 UT on 1 November 2012 (the second vertical green line in Figure 1i), which is driven by the MC body attributing to the prolonged strong southward magnetic field inside lasting for >20 hr (Gonzalez et al., 1994).

Figure 2 shows the presence and interruption of the dropout of the radiation belt energetic electron flux at seven typical energy channels from 103 keV to 2.6 MeV for different L-shells at a 90° local pitch angle observed by Van Allen Probe -A and -B from 31 October to 2 November 2012. The locations of the magnetopause and calculated last closed drift shell (LCDS) were estimated by following Shue et al. (1997) and LANLGeoMag library (e.g., Albert et al., 2018) as shown in Figure 2c. During the prolonged initial phase, both the magnetopause was moved inward to lower L^* when the dynamic pressure stayed at a high level. During the storm main phase, the magnetopause location moved outwards as the solar wind dynamic pressure became lower while LCDS continued moving to lower L-shells. The loss of ultra-relativistic electron fluxes (>1.5 MeV, Figures 2g–2j) at high L shells during the entire event mainly underwent a two-step dropout. During the initial phase, a rapid loss was observed at

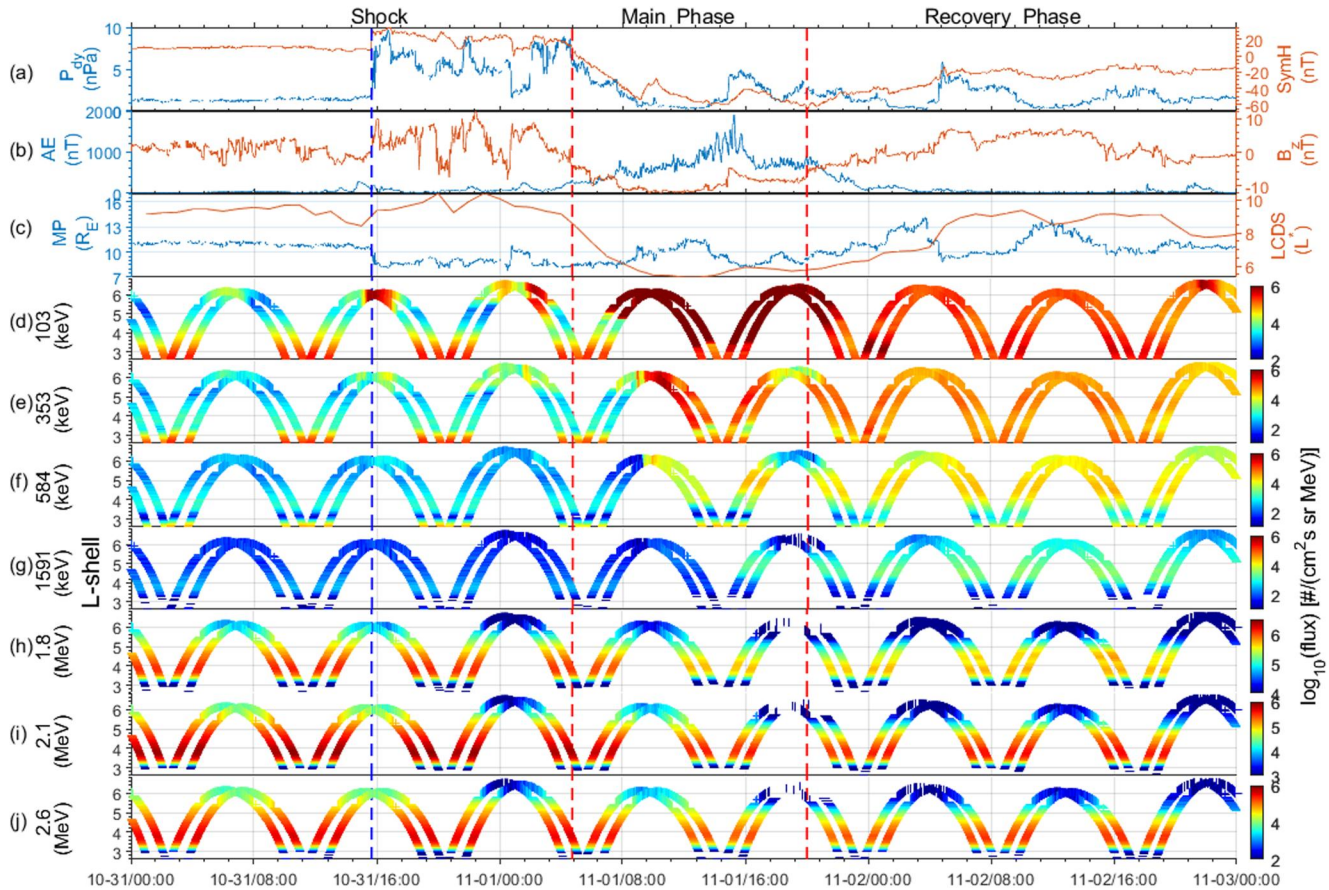

Figure 2. A schematic of radiation belt flux loss from 31 October to 2 November 2012. From top to bottom: (a) the solar wind dynamic pressure (blue) and SymH index (red); (b) AE index (blue) and Bz (red) in GSE; (c) magnetopause location (blue) and last closed drift shell (red); (d)–(j) Van-A and Van-B observed the flux variation of 90° local pitch angle at different L-shell. The energy channels are (d) 103 keV, (e) 353 keV, (f) 584 keV, (g) 1,591 keV, (h) 1.8 MeV, (i) 2.1 MeV, and (j) 2.6 MeV.

high L shells when the dynamic pressure consistently remained at a high value. Since this loss mainly occurred in more than one period of spacecraft orbit (~9 hr) after the IP shock, it could be suggested that the persistent high dynamic pressure could be the probable candidate that accounted for the electron depletion. Immediately after the onset of the storm main phase when AE (Figure 2b) increased and interplanetary magnetic field (IMF) Bz (Figure 2a) turned southward, which indicated the occurrence of a substorm. Then the electron loss process was interrupted with a clear flux enhancement at high L shells, called the interruption region where the dropout process is interrupted by the local acceleration of electrons by the chorus waves, which can drastically change the spatial distribution of the radiation belt electrons. A few hours later, a more significant electron dropout could be observed at high L shells at the end of the storm main phase when SymH arrived around its minimum. For lower electron energies (584 and 1,591 keV), the loss of electrons became weaker, while the interruption (i.e., enhancement of electron fluxes) became more pronounced and penetrated into the core of the outer radiation belt, as shown in Figures 2f–2g. For electrons at low energies (103 and 353 keV, Figures 2d–2e), clear depletion occurred at high L shells in the initial phase followed by a distinct enhancement at a broader range of L shells ($L^* > 3$), while loss in the main phase was absent. By comparing the temporal variation of electron fluxes in different stages of the event, it can be suggested that the generation and interruption of electron loss have a close relationship with the dynamic pressure, geomagnetic storm, and substorm activities. A detailed analysis of the loss and source of radiation belt electrons in response to the solar wind disturbance in this event will be given in the rest of our article.

To remove the adiabatic variations of electron fluxes, we show the temporal evolution of relativistic electron PSD distributions for fixed $K = 0.17\ G^{1/2}R_E$ (corresponding roughly to ~30° to 40° pitch angle for a dipole field) with μ = 2,290 MeV/G (corresponding roughly to ~2.3 MeV at L = 4.5 or 3 MeV at L = 4.0 for a dipole field) at

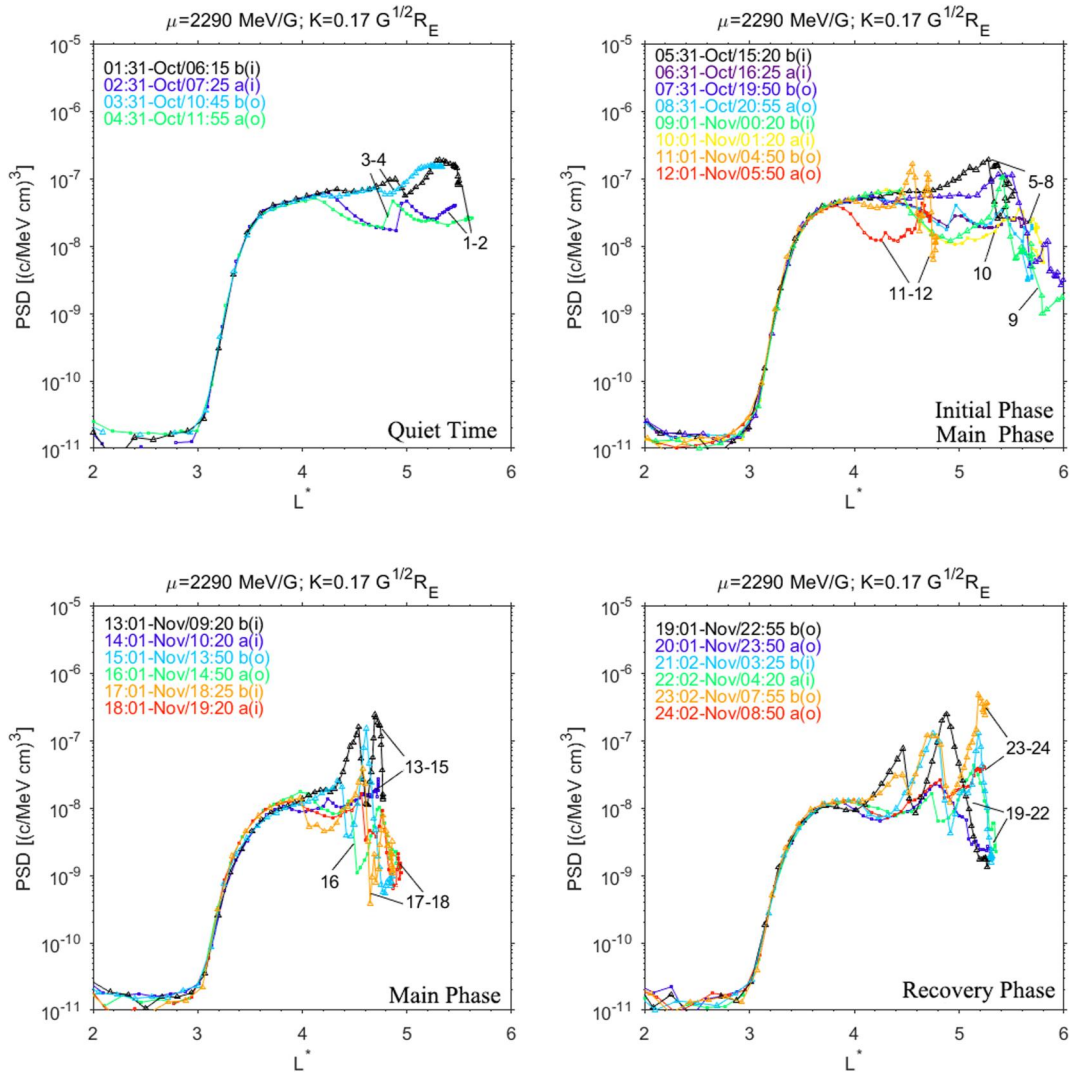

Figure 3. Relativistic electron phase space density (PSD) distributions at different L^* for fixed $K = 0.17\ G^{1/2}R_E$ and $\mu = 2{,}290$ MeV/G. The four Subgraphs correspond to PSD variations in different phases. Different colors in each subgraph correspond to the start time of inbound (i) or outbound (o) orbit passes from both VAP-A (squares) and VAP-B (triangles). Each curve was numbered for ease of identification.

different L^* in Figure 3. When the IP shock arrived at the magnetosphere at 15:40 UT (the shifted time of the solar wind data is 70 min), VAP-B was located at $L^* = 5.37$ in its inbound trajectory (curve 5), while VAP-A was at $L^* = 5.62$ in its outbound trajectory (curve 6). Thus, we can briefly consider curve 7 as the beginning of the event. Similar to the electron flux observations in Figure 2, the PSD at large L shells ($L^* > 4.5$) decreased gradually by more than one order of magnitude a few hours after the IP shock while the dynamic pressure maintained a high value (curves 7–10). At the onset of the storm main phase (curves 11–12), the dropout penetrated the deeper region at $L^* = \sim 4$ with a continuous decrease of PSD by one order of magnitude and an obvious cutoff at $L^* = \sim 4.8$, which is consistent with the finding that the PSD continuously decreases and forms an obvious cutoff at the onset of the storm main phase (e.g., Turner et al., 2014). However, it is interesting that a PSD peak appeared around $L^* = 4.5$ and lasted for 15 hr, with a maximum value of more than one order larger than that at $L^* = \sim 4$. This indicates a multiple peak structure of a relativistic electron radiation belt (e.g., Pinto et al., 2018). As the geomagnetic storm intensified and the SymH continued decreasing, the electron PSD kept declining (curves 13–18). Nevertheless, the multiple peak structures of the radiation belt remained distinct throughout the main phase. During the recovery phase (curves 19–24), the "slot region" between the two peaks was filled up and the electron PSD at $L^* > 4$ recovered to pre-event level or higher. It suggests that an additional source process of the

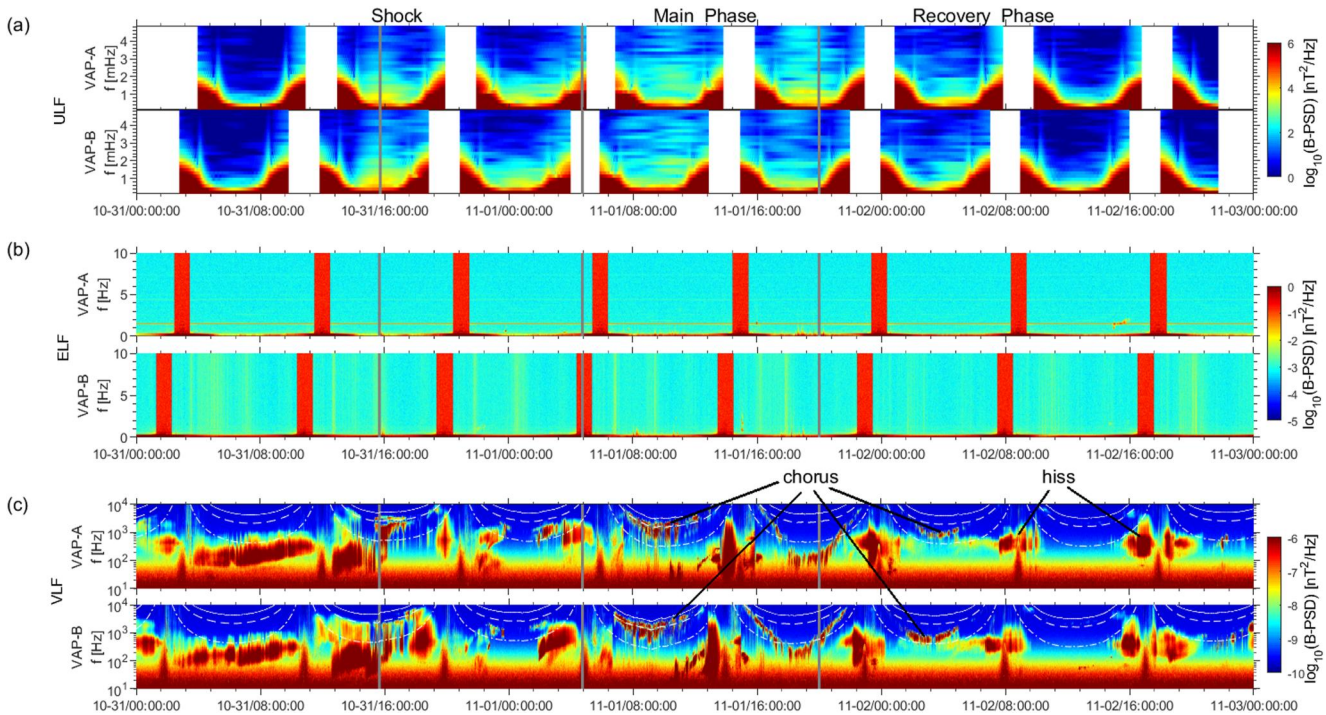

Figure 4. Temporal evolutions of the magnetic power spectral density of (a) ULF waves at 1–5 mHz; (b) ELF waves at 0–10 Hz; and (c) VLF waves including chorus and hiss at 10–10^4 Hz are observed using VAP-A and VAP-B, respectively.

relativistic electron should exist both during the main phase and during the recovery phase to counteract the electron dropout processes in the heart of the radiation belt (L^* = 4–5).

4. Discussions

The population and energies in the outer radiation belt are usually redistributed by various effects triggered by MC-magnetosphere couplings. One of the most crucial mechanisms is the wave-particle interactions which can potentially increase or decrease radiation belt electrons when dynamic pressure rises and geomagnetic storms or substorms happen. We combine waves in three specific frequency ranges, that is, the Ultra-Low Frequency waves (ULF, 1–5 mHz), the Extremely Low Frequency waves (ELF, 0–10 Hz), and the Very-Low Frequency waves (VLF, 10–10000 Hz). The ULF waves are usually generated in the frequency range of Pc5 when Earth's magnetosphere is compressed by the solar wind. The waves are capable of breaking the third adiabatic invariants of radiation belt electrons by drift resonance, thus leading to the radial transport of the electrons. As shown in Figure 4a, the ULF waves enhanced across the shock and persisted during the main phase. It indicates that the outward radial diffusions driven by ULF waves were a potential candidate for the outward transportation of electrons, thus leading the rapid loss both in the initial phase and in the main phase. Within the prolonged initial phase, the high solar wind dynamic pressure could continue moving the magnetopause to lower L^* and strengthen the magnetopause shadowing effect. The probable process could be that the persistent high dynamic pressure combined with ULF-driven outward transport preferentially causes the decrease of the electron PSD at higher L shells. During the storm main phase, as shown in Figure 2c, the magnetopause location moved outwards as the solar wind dynamic pressure became lower. It can be suggested that the magnetopause shadowing effect or the "PSD cutoff effect" was weaker. However, the LCDS moved to a much lower location due to the decreasing Dst with IMF Bz turning south, thus the ULF-driven outward transport could be the more important to lead to the magnetopause loss. An alternative relativistic electron dropout effect is the local loss to the atmosphere. It is reported that the EMIC waves could scatter radiation belt relativistic electrons loss into Earth's atmosphere via pitch angle resonance during geomagnetic storms or substorms. The EMIC waves can be classified as Pc1-2 waves (0.1–5.0 Hz in the outer radiation belt) and are commonly excited by the instability of substorm-inject hot protons, oxygen, or helium (Zhang, Li, Thorne, Angelopoulos, Bortnik, et al., 2016). Figure 4b shows the

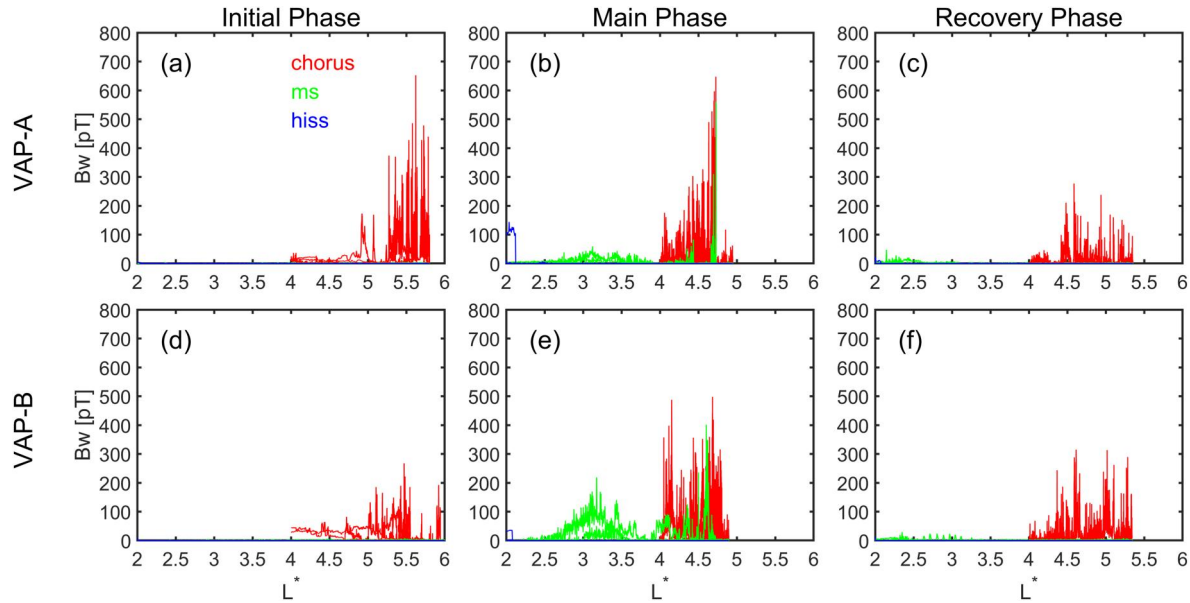

Figure 5. Wave magnetic amplitude (Bw) of the chorus (red), ms (green), and hiss (blue) as a function of L^* during the initial phase and main phase recovery phase of the geomagnetic storm observed from VAP-A and VAP-B, respectively.

ELF wave spectrum from 0 to 10 Hz which covers the whole frequency range of EMIC waves. However, the EMIC waves can hardly be found in Figure 4b. Moreover, no distinct local minimum of relativistic electron PSD can be detected during the main phase (see Figure 3). It is indicated that EMIC-driven loss could not be the main reason for the electron PSD dropout. It can be concluded that the relativistic electron PSD dropout during the initial phase and the main phase was mainly caused by both the persistent dynamic pressure and the ULF-driven outward transport.

Figure 4c presents the occurrence of the magnetic power spectral density of whistler mode chorus, plasmaspheric hiss, and magnetosonic (ms) waves before and during the MC event. To compare their spatial distribution, the superposed integrated wave magnetic amplitude (Bw) along with L^* (calculated with $K = 0.17\ \mathrm{G}^{1/2}R_\mathrm{E}$ and $\mu = 2{,}290$ MeV/G) during the initial phase, main phase, and recovery phase of the geomagnetic storm is illustrated in Figure 5. Intense chorus waves can be distinctly found at $L^* > 5$ (Figures 5a and 5d) with a peak value around $L^* = 5.5$ in the initial phase, indicating the possible wave environment to accelerate seed electrons to relativistic electrons. However, the observations of local flux and PSD change of electrons (Figures 2 and 3) demonstrate that the possible accelerations via wave-particle interactions were too weak compared with the rapid loss mechanisms at higher L-shells. During the main phase (Figures 5b and 5e) when the dynamic pressure became weak, chorus waves intensified and were mainly present between $L^* = 4$–5. The amplitude of the waves can be up to 700 pT around $L^* = 4.5$, as shown in Figure 5b. This maximum location of the wave amplitude is remarkably consistent with the observed peak location of the relativistic electron PSD during the main phase, as shown in curves 11–17 in Figure 3. It can be suggested that the chorus-led accelerations account for the local peak of relativistic electron PSD. During the recovery phase, the chorus waves became weak but distributed at a broader range of L^* (4.0–5.5) when the PSD of the relativistic electron was bumped up to the pre-event level or higher. The probable scenario process of generation and interruption would be as below:

1. During the initial phase, the persistent high dynamic pressure caused the magnetosphere's strong compression and excited ULF waves, which caused the magnetopause shadowing combined with the outward transportations to drop out of the radiation belt relativistic electrons into interplanetary space within a few hours.
2. During the main phase, the continuous ULF waves kept decreasing the electrons while the magnetosphere moved outwards as the dynamic pressure became comparably weaker. Therefore, the magnetopause shadowing was theoretically harder to cause the electron loss. On the other hand, enhanced whistler-mode chorus waves excited by substorm injections locally accelerated the seed electrons via wave-particle interactions

around the heart of the outer radiation belt, thus overcoming the magnetopause shadowing, that is, interrupting the loss processes, and showing a multiple peak radiation belt for relativistic electrons.
3. During the recovery phase, the loss processes of the electrons became much weaker while the chorus-dominated acceleration continued at a broader range, resulting in the total PSD recovering to the pre-storm level or higher.

In addition, groups of ms waves were also found at $L^* = 2.5$–4.5 with Bw up to 300 pT as well as hiss waves appearing at $L^* < 2.5$ with Bw close to 100 pT in the storm main phase (Figures 5b and 5e). However, both of them can hardly theoretically deplete or accelerate the relativistic electrons within a few hours (e.g., Bortnik & Thorne, 2010; Ripoll et al., 2016).

5. Summary

In this study, we completely analyzed and discussed the generation and interruption of relativistic electron PSD dropout in the heart of the Earth radiation belt ($L^* = 4$–5) caused by a MC event that impinged the Earth's magnetosphere on 31 October 2012 and caused a moderate geomagnetic storm. The MC-driven shock triggered the storm SSC, the sheath region and the front part of the MC body with long-lasting high dynamic pressure and roughly northward magnetic field drove a special prolonged initial phase lasting for >13 hr, and the persistent strong southward magnetic fields inside the MC body were responsible for the storm main phase. By comparing the variations in the electron PSD and wave power distributions during the passage of different parts of this MC event, the following conclusions can be drawn:

1. Persistent high dynamic pressure and excited ULF waves dominated the rapid loss of radiation belt relativistic electron PSD at $L^* > 4$ during the storm initial phase, regardless of the acceleration process induced by the whistler-mode chorus, which was too weak to confront the loss.
2. The acceleration process led by the chorus via wave-particle resonance at $L^* = 4$–5.5 took over the variation of relativistic electrons, thus totally interrupting the loss processes during the storm main phase and recovery phase, as dynamic pressure decreased, and chorus waves intensified.
3. The competition between the interplanetary loss and chorus wave-led acceleration processes caused the commencement and interruption of the relativistic electrons PSD dropout process in the heart of the outer radiation belt, which would be valuable to take into special consideration in further investigations of MC-radiation belt coupling.
4. By triggering magnetosphere shadowing and substorm particle injections, special solar wind conditions including the sheath with persistent high dynamic pressure and the MC body with strong southward magnetic field dominate the balance of the loss and acceleration processes in the heart of the outer radiation belt.

Data Availability Statement

The Wind MFI and SWE data and geomagnetic indices are available at NASA OmniWeb (http://cdaweb.gsfc.nasa.gov). The REPT and MagEIS data are obtained from https://spdf.gsfc.nasa.gov/pub/data/rbsp. The EMFISIS data are derived from https://emfisis.physics.uiowa.edu/data/index.

Acknowledgments
This work is jointly supported by National Key Research and Development Program of China (Grant 2022YFF0503904), the National Natural Science Foundation of China (Grant 42074205), Guangdong Basic and Applied Basic Research Foundation (Grant 2023B1515040021), Hong Kong-Macao Exchange Project of Harbin Institute of Technology, Shenzhen Key Laboratory Launching Project (Grant ZDSYS20210702140800001), and the Science and Technology Development Fund of Macao SAR (File No. 0048/2021/A).

References

Albert, J. M., Selesnick, R. S., Morley, S. K., Henderson, M. G., & Kellerman, A. C. (2018). Calculation of last closed drift shells for the 2013 GEM radiation belt challenge events. *Journal of Geophysical Research: Space Physics*, *123*(11), 9597–9611. https://doi.org/10.1029/2018JA025991

Allison, H. J., Shprits, Y. Y., Zhelavskaya, I. S., Wang, D., & Smirnov, A. G. (2021). Gyroresonant wave-particle interactions with chorus waves during extreme depletions of plasma density in the Van Allen radiation belts. *Science Advances*, *7*(5), eabc0380. https://doi.org/10.1126/sciadv.abc0380

Baker, D. N., Kanekal, S. G., Hoxie, V. C., Batiste, S., Bolton, M., Li, X., et al. (2013). The relativistic electron-proton telescope (REPT) instrument on board the radiation belt storm probes (RBSP) spacecraft: Characterization of Earth's radiation belt high-energy particle populations. *Space Science Reviews*, *179*(1–4), 337–381. https://doi.org/10.1007/s11214-012-9950-9

Blake, J. B., Carranza, P. A., Claudepierre, S. G., Clemmons, J. H., Crain, W. R., Dotan, Y., et al. (2013). The magnetic electron ion spectrometer (MagEIS) instruments aboard the radiation belt storm probes (RBSP) spacecraft. *Space Science Reviews*, *179*(1–4), 383–421. https://doi.org/10.1007/s11214-013-9991-8

Borovsky, J. E., & Denton, M. H. (2006). Differences between CME-driven storms and CIR-driven storms. *Journal of Geophysical Research*, *111*(A7), A07S08. https://doi.org/10.1029/2005JA011447

Bortnik, J., & Thorne, R. M. (2010). Transit time scattering of energetic electrons due to equatorially confined magnetosonic waves. *Journal of Geophysical Research*, *115*(A7). https://doi.org/10.1029/2010JA015283

Chen, Y., Reeves, G. D., & Friedel, R. H. W. (2007). The energization of relativistic electrons in the outer Van Allen radiation belt. *Nature Physics*, *3*(9), 614–617. https://doi.org/10.1038/nphys655

Gao, X., Lu, Q., Bortnik, J., Li, W., Chen, L., & Wang, S. (2016). Generation of multiband chorus by lower band cascade in the Earth's magnetosphere. *Geophysical Research Letters*, *43*(6), 2343–2350. https://doi.org/10.1002/2016GL068313

Gonzalez, W. D., Joselyn, J. A., Kamide, Y., Kroehl, H. W., Rostoker, G., Tsurutani, B. T., & Vasyliunas, V. M. (1994). What is a geomagnetic storm? *Journal of Geophysical Research*, *99*(A4), 5771–5792. https://doi.org/10.1029/93JA02867

Hao, Y. X., Zong, Q.-G., Zhou, X.-Z., Rankin, R., Chen, X. R., Liu, Y., et al. (2017). Relativistic electron dynamics produced by azimuthally localized poloidal mode ULF waves: Boomerang-shaped pitch angle evolutions. *Geophysical Research Letters*, *44*(15), 7618–7627. https://doi.org/10.1002/2017GL074006

Horne, R. B., Thorne, R. M., Glauert, S. A., Albert, J. M., Meredith, N. P., & Anderson, R. R. (2005). Timescale for radiation belt electron acceleration by whistler mode chorus waves. *Journal of Geophysical Research*, *110*(A3), A03225. https://doi.org/10.1029/2004JA010811

Kletzing, C. A., Kurth, W. S., Acuna, M., MacDowall, R. J., Torbert, R. B., Averkamp, T., et al. (2013). The electric and magnetic field instrument suite and integrated science (EMFISIS) on RBSP. *Space Science Reviews*, *179*(1–4), 127–181. https://doi.org/10.1007/s11214-013-9993-6

Lepping, R. P., Acũna, M. H., Burlaga, L. F., Farrell, W. M., Slavin, J. A., Schatten, K. H., et al. (1995). The WIND magnetic field investigation. *Space Science Reviews*, *71*(1–4), 207–229. https://doi.org/10.1007/BF00751330

Li, J., Bortnik, J., An, X., Li, W., Angelopoulos, V., Thorne, R. M., et al. (2019). Origin of two-band chorus in the radiation belt of Earth. *Nature Communications*, *10*(1), 4672. https://doi.org/10.1038/s41467-019-12561-3

Li, W., Bortnik, J., Thorne, R. M., & Angelopoulos, V. (2011). Global distribution of wave amplitudes and wave normal angles of chorus waves using THEMIS wave observations. *Journal of Geophysical Research*, *116*(A12). https://doi.org/10.1029/2011JA017035

Li, W., Thorne, R. M., Ma, Q., Ni, B., Bortnik, J., Baker, D. N., et al. (2014). Radiation belt electron acceleration by chorus waves during the 17 March 2013 storm. *Journal of Geophysical Research: Space Physics*, *119*(6), 4681–4693. https://doi.org/10.1002/2014JA019945

Ma, Q., Mourenas, D., Artemyev, A., Li, W., Thorne, R. M., & Bortnik, J. (2016). Strong enhancement of 10–100 keV electron fluxes by combined effects of chorus waves and time domain structures. *Geophysical Research Letters*, *43*(10), 4683–4690. https://doi.org/10.1002/2016GL069125

Morley, S. K., Friedel, R. H. W., Spanswick, E. L., Reeves, G. D., Steinberg, J. T., Koller, J., et al. (2010). Dropouts of the outer electron radiation belt in response to solar wind stream interfaces: Global positioning system observations. *Proceedings of the Royal Society A: Mathematical, Physical and Engineering Sciences*, *466*(2123), 3329–3350. https://doi.org/10.1098/rspa.2010.0078

Moya, P. S., Pinto, V. A., Sibeck, D. G., Kanekal, S. G., & Baker, D. N. (2017). On the effect of geomagnetic storms on relativistic electrons in the outer radiation belt: Van Allen probes observations. *Journal of Geophysical Research: Space Physics*, *122*(11). https://doi.org/10.1002/2017JA024735

Ni, B., Cao, X., Zou, Z., Zhou, C., Gu, X., Bortnik, J., et al. (2015). Resonant scattering of outer zone relativistic electrons by multiband EMIC waves and resultant electron loss time scales. *Journal of Geophysical Research: Space Physics*, *120*(9), 7357–7373. https://doi.org/10.1002/2015JA021466

Ni, B., Shprits, Y., Nagai, T., Thorne, R., Chen, Y., Kondrashov, D., & Kim, H. (2009). Reanalyses of the radiation belt electron phase space density using nearly equatorial CRRES and polar-orbiting Akebono satellite observations. *Journal of Geophysical Research*, *114*(A5), 2008JA013933. https://doi.org/10.1029/2008JA013933

Ogilvie, K. W., Chornay, D. J., Fritzenreiter, R. J., Hunsaker, F., Keller, J., Lobell, J., et al. (1995). SWE, a comprehensive plasma instrument for the WIND spacecraft. *Space Science Reviews*, *71*(1–4), 55–77. https://doi.org/10.1007/BF00751326

Pinto, V. A., Bortnik, J., Moya, P. S., Lyons, L. R., Sibeck, D. G., Kanekal, S. G., et al. (2018). Characteristics, occurrence, and decay rates of Remnant belts associated with three-belt events in the Earth's radiation belts. *Geophysical Research Letters*, *45*(22). https://doi.org/10.1029/2018GL080274

Reeves, G. D., Spence, H. E., Henderson, M. G., Morley, S. K., Friedel, R. H. W., Funsten, H. O., et al. (2013). Electron acceleration in the heart of the Van Allen radiation belts. *Science*, *341*(6149), 991–994. https://doi.org/10.1126/science.1237743

Ripoll, J.-F., Loridan, V., Cunningham, G. S., Reeves, G. D., & Shprits, Y. Y. (2016). On the time needed to reach an equilibrium structure of the radiation belts. *Journal of Geophysical Research: Space Physics*, *121*(8), 7684–7698. https://doi.org/10.1002/2015JA022207

Shprits, Y. Y., Thorne, R. M., Friedel, R., Reeves, G. D., Fennell, J., Baker, D. N., & Kanekal, S. G. (2006). Outward radial diffusion driven by losses at magnetopause. *Journal of Geophysical Research*, *111*(A11), A11214. https://doi.org/10.1029/2006JA011657

Shue, J.-H., Chao, J. K., Fu, H. C., Russell, C. T., Song, P., Khurana, K. K., & Singer, H. J. (1997). A new functional form to study the solar wind control of the magnetopause size and shape. *Journal of Geophysical Research*, *102*(A5), 9497–9511. https://doi.org/10.1029/97JA00196

Su, Z., Gao, Z., Zheng, H., Wang, Y., Wang, S., Spence, H. E., et al. (2017). Rapid loss of radiation belt relativistic electrons by EMIC waves. *Journal of Geophysical Research: Space Physics*, *122*(10), 9880–9897. https://doi.org/10.1002/2017JA024169

Summers, D., Ma, C., Meredith, N. P., Horne, R. B., Thorne, R. M., Heynderickx, D., & Anderson, R. R. (2002). Model of the energization of outer-zone electrons by whistler-mode chorus during the October 9, 1990 geomagnetic storm. *Geophysical Research Letters*, *29*(24), 27-1–27-4. https://doi.org/10.1029/2002GL016039

Tsyganenko, N. A., & Sitnov, M. I. (2005). Modeling the dynamics of the inner magnetosphere during strong geomagnetic storms. *Journal of Geophysical Research*, *110*(A3), A03208. https://doi.org/10.1029/2004JA010798

Turner, D. L., Shprits, Y., Hartinger, M., & Angelopoulos, V. (2012). Explaining sudden losses of outer radiation belt electrons during geomagnetic storms. *Nature Physics*, *8*(3), 208–212. https://doi.org/10.1038/nphys2185

Turner, D. L., & Ukhorskiy, A. Y. (2020). Outer radiation belt losses by magnetopause incursions and outward radial transport: New insight and outstanding questions from the Van Allen Probes era. In *The dynamic loss of Earth's radiation belts* (pp. 1–28). Elsevier. https://doi.org/10.1016/B978-0-12-813371-2.00001-9

Turner, D. L., Angelopoulos, V., Morley, S. K., Henderson, M. G., Reeves, G. D., Li, W., et al. (2014). On the cause and extent of outer radiation belt losses during the 30 September 2012 dropout event: Effective ranges of outer belt dropouts. *Journal of Geophysical Research: Space Physics*, *119*(3), 1530–1540. https://doi.org/10.1002/2013JA019446

Turner, D. L., Kilpua, E. K. J., Hietala, H., Claudepierre, S. G., O'Brien, T. P., Fennell, J. F., et al. (2019). The response of Earth's electron radiation belts to geomagnetic storms: Statistics from the Van Allen Probes era including effects from different storm drivers. *Journal of Geophysical Research: Space Physics*, *124*(2), 1013–1034. https://doi.org/10.1029/2018JA026066

Turner, D. L., Morley, S. K., Miyoshi, Y., Ni, B., & Huang, C.-L. (2013). Outer radiation belt flux dropouts: Current understanding and unresolved questions. In D. Summers, I. R. Mann, D. N. Baker, & M. Schulz (Eds.), *Geophysical monograph series* (pp. 195–212). American Geophysical Union. https://doi.org/10.1029/2012GM001310

Xiang, Z., Tu, W., Li, X., Ni, B., Morley, S. K., & Baker, D. N. (2017). Understanding the mechanisms of radiation belt dropouts observed by Van Allen Probes. *Journal of Geophysical Research: Space Physics*, *122*(10), 9858–9879. https://doi.org/10.1002/2017JA024487

Zhang, X.-J., Li, W., Thorne, R. M., Angelopoulos, V., Bortnik, J., Kletzing, C. A., et al. (2016). Statistical distribution of EMIC wave spectra: Observations from Van Allen Probes. *Geophysical Research Letters*, *43*(24). https://doi.org/10.1002/2016GL071158

Zhang, X.-J., Li, W., Thorne, R. M., Angelopoulos, V., Ma, Q., Li, J., et al. (2016). Physical mechanism causing rapid changes in ultrarelativistic electron pitch angle distributions right after a shock arrival: Evaluation of an electron dropout event. *Journal of Geophysical Research: Space Physics*, *121*(9), 8300–8316. https://doi.org/10.1002/2016JA022517

Zhao, H., & Li, X. (2013). Inward shift of outer radiation belt electrons as a function of Dst index and the influence of the solar wind on electron injections into the slot region. *Journal of Geophysical Research: Space Physics*, *118*(2), 756–764. https://doi.org/10.1029/2012JA018179

Zou, Z., Zuo, P., Ni, B., Gao, Z., Wang, G., Zhao, Z., et al. (2020). Two-step dropouts of radiation belt electron phase space density induced by a magnetic cloud event. *The Astrophysical Journal*, *895*(1), L24. https://doi.org/10.3847/2041-8213/ab9179